ISSN 1674-1056
http://cpb.iphy.ac.cn
http://iopscience.iop.org/cpb
中国物理 B
Chinese Physics
中国物理
Chinese Physics B

Mask-based denoising scheme for ghost imaging

Yang Zhou(周阳), Shu-Xu Guo(郭树旭), Fei Zhong(钟菲), Tian Zhang(张天)

Citation: Chin. Phys. B . 2019, 28(8): 084204. **doi:** 10.1088/1674-1056/28/8/084204
Journal homepage: http://cpb.iphy.ac.cn; http://iopscience.iop.org/cpb

What follows is a list of articles you may be interested in

Enhancement of spatial resolution of ghost imaging via localizing and thresholding

Yunlong Wang(王云龙), Yingnan Zhou(周英男), Shaoxiong Wang(王少雄), Feiran Wang(王斐然), Ruifeng Liu(刘瑞丰), Hong Gao(高宏), Pei Zhang(张沛), Fuli Li(李福利)
Chin. Phys. B . 2019, 28(4): 044202. **doi:** 10.1088/1674-1056/28/4/044202

Reflective ghost imaging free from vibrating detectors

Heng-xing Li(李恒星), Yan-feng Bai(白艳锋), Xiao-hui Shi(施晓辉), Su-qin Nan(南苏琴), Li-jie Qu(屈利杰), Qian Shen(沈倩), Xi-quan Fu(傅喜泉)
Chin. Phys. B . 2017, 26(10): 104204. **doi:** 10.1088/1674-1056/26/10/104204

Optical encryption scheme based on ghost imaging with disordered speckles

Yu-dong Zhang(张玉东), Sheng-mei Zhao(赵生妹)
Chin. Phys. B . 2017, 26(5): 054205. **doi:** 10.1088/1674-1056/26/5/054205

Lensless ghost imaging through the strongly scattering medium

Zhe Yang(杨哲), Lianjie Zhao(赵连洁), Xueliang Zhao(赵学亮), Wei Qin(秦伟), Junlin Li(李俊林)
Chin. Phys. B . 2016, 25(2): 024202. **doi:** 10.1088/1674-1056/25/2/024202

Increasing the range accuracy of three-dimensional ghost imaging ladar using optimum slicing number method

Yang Xu, Zhang Yong, Xu Lu, Yang Cheng-Hua, Wang Qiang, Liu Yue-Hao, Zhao Yuan
Chin. Phys. B . 2015, 24(12): 124202. **doi:** 10.1088/1674-1056/24/12/124202

Mask-based denoising scheme for ghost imaging*

Yang Zhou(周阳)[1], Shu-Xu Guo(郭树旭)[1], Fei Zhong(钟菲)[2], and Tian Zhang(张天)[3,†]

[1] *State Key Laboratory on Integrated Optoelectronics, College of Electronic Science and Engineering, Jilin University, Changchun* 130012, *China*
[2] *Changchun Institute of Technology, School of Electrical Engineering and Information Technology, Changchun* 130012, *China*
[3] *School of Physics, Northeast Normal University, Changchun* 130024, *China*

(Received 22 February 2019; revised manuscript received 9 April 2019; published online 9 July 2019)

Ghost imaging (GI) is thought of as a promising imaging method in many areas. However, the main drawback of GI is the huge measurement data and low signal-to-noise ratio. In this paper, we propose a novel mask-based denoising scheme to improve the reconstruction quality of GI. We first design a mask through the maximum between-class variance (OTSU) method and construct the measurement matrix with speckle patterns. Then, the correlated noise in GI can be effectively suppressed by employing the mask. From the simulation and experimental results, we can conclude that our method has the ability to improve the imaging quality compared with traditional GI method.

Keywords: ghost imaging, maximum between-class variance, mask, image quality

PACS: 42.30.Va, 42.30.Wb **DOI:** 10.1088/1674-1056/28/8/084204

1. Introduction

In recent years, ghost imaging (GI) has attracted considerable attention due to its ability to reconstruct an unknown object through spatial intensity correlation measurements from tow detectors. Unlike the traditional imaging methods, one of the detectors without spatial resolution is needed in ghost imaging to contain the object information. The other detector with spatial resolution is employed to detect the light source. Quantum ghost imaging was first theoretically introduced by Klyshko and demonstrated experimentally by Pittman[1,2] in 1995. Afterwards, it was discovered that pseudo-thermal light sources[3–5] and thermal light sources[6] can be exploited to achieve GI. Now, researchers are working towards the progress from pure theory to real-world applications.

Recent research has revealed that GI has received increasing attention due to its novel physical characteristics, such as non-lens imaging, atmospheric turbulence free, *etc*.[7–10] These studies demonstrated that GI is a very powerful tool for imaging objects in optically harsh fields such as lidar detection, three-dimensional (3D) imaging, biomedical imaging, *etc*.[11–23] Unfortunately, the limitation of signal-to-noise ratio (SNR) and resolution are an obstacle for GI to use pseudo-thermal light, which is difficult to meet practical application requirements. Therefore, improving GI image quality with fewer measurements is the crucial problem to be resolved. In order to address this issue, many novel reconstruction methods have been proposed.[24–35] In Ref. [24], the normalized ghost imaging (NGI) with a more appropriate weighting factor is applied to the ensemble average of the estimated object, and has a similar performance to the differential ghost imaging (DGI).[25] Besides, the iterative denoising of ghost imaging (IDGI)[26–28] shows a remarkable enhancement in terms of reconstruction quality by estimating the noise terms via the conventional GI algorithm. However, the IDGI relies on the quality of the original GI reconstruction image. Comparing with the above methods, the reconstruction quality of compressive-sensing ghost imaging (CGI)[29–32] shows significant improvement and lower measurements than Nyquist sampling limit. However, it may rely on the prior character of the object, and the optimization procedure itself is time-consuming and memory-wasting. Though pseudo-inverse GI (PGI)[33,34] is likely to enhance the visibility and spatial resolution of GI with respect to the property of the pseudo-inverse matrix, it cannot acquire the robust images in practical engineering applications. Instead of optimizing the speckle pattern, scalar-matrix-structured[35] GI demonstrates a robust reconstruction image. However, this method lacks universality in practical applications and does not give a method of constructing an effective scalar matrix either.

In this paper, a mask-based denoising ghost imaging (MDGI) method is proposed, which aims to remove the correlated noise in GI and improving the quality of the reconstructed image. This method has better imaging quality than DGI and NGI. Compared with IDGI, it does not depend on the quality of the original GI methods. Compared with the SMGI method, an effective construction method of the new measurement matrix is given. Firstly, we theoretically analyze

*Project supported by the National Natural Science Foundation of China (Grant No. 61627823), the Foundation for Excellent Young Talents of Jilin Province, China (Grant No. 20190103010JH), the "13th Five-Year" Science and Technology Research Project of the Education Department of Jilin Province, China (Grant No. JJKH20190277KJ), the China Postdoctoral Science Foundation (Grant No. 2018M641759), and the Fundamental Research Funds for the Central Universities, China (Grant No. 2412018QD002).

†Corresponding author. E-mail: zhangtian114@sina.cn

© 2019 Chinese Physical Society and IOP Publishing Ltd

the reason why the SNR of DGI and NGI are both higher than that of GI. Then, we use the OTSU[36] method to calculate the optimal threshold corresponding to the correlated noise in GI. Finally, the mask is obtained by combining the calculated optimal threshold with that from a dilation method, and it is used to further reduce the correlated noise in GI. From simulations and experimental results, we can conclude that our method can effectively remove the correlated noise in GI and improve the imaging quality index compared with GI, DGI and NGI method.

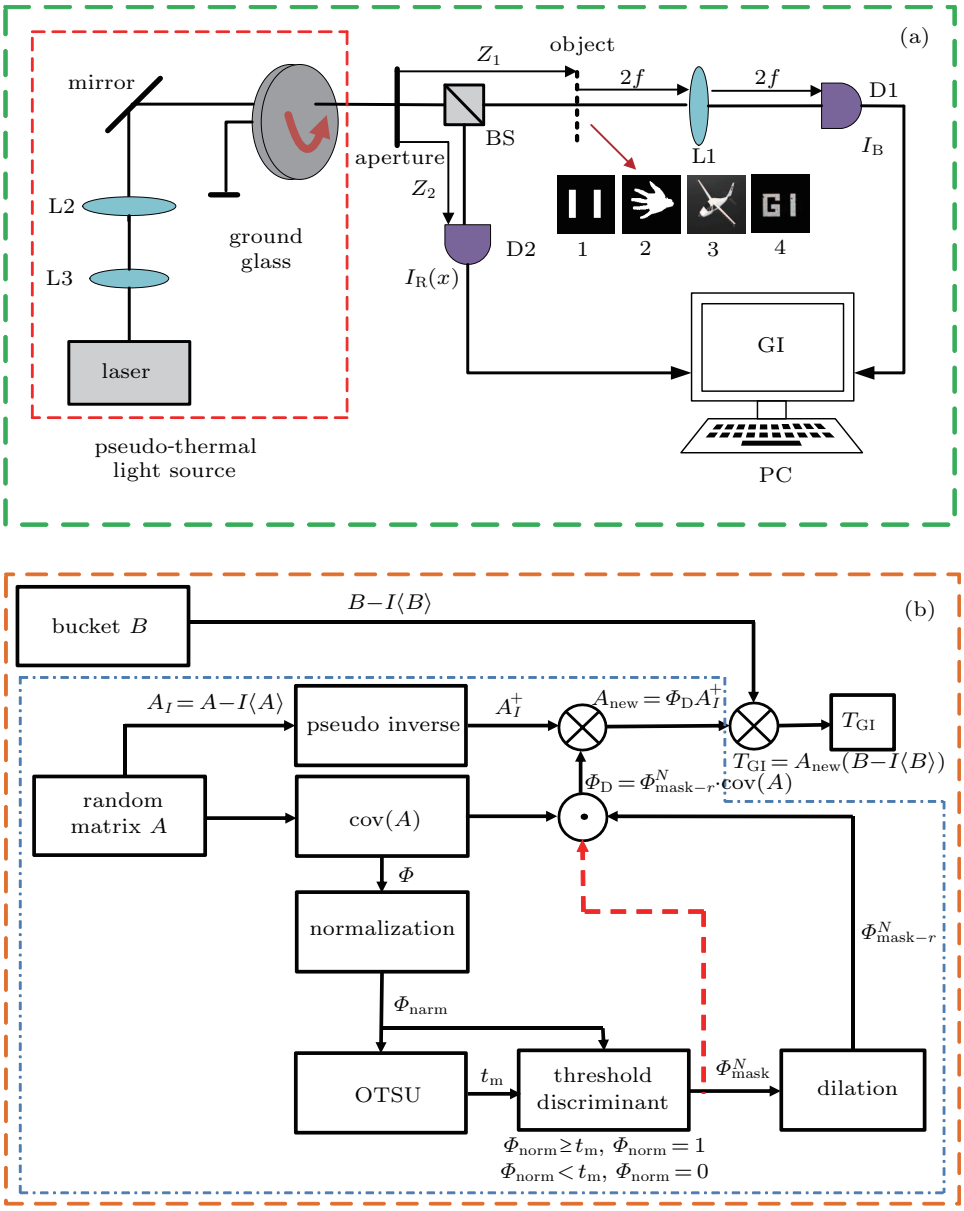


Fig. 1. Schematic diagram of MDGI with pseudo thermal light. (a) Schematic diagram of ghost imaging with pseudo thermal light. Inside the red dotted line on the left side of the schematics is pseudo-thermal light source. BS: beam splitter; D1: bucket detector without spatial resolution; D2: reference detector with spatial resolution; L: lens; Z_1: distance between light source and object; Z_2: distance between light source and reference detector; PC: personal computer. (b) Schematic diagram of mask-based denoising scheme. Inside the blue dotted line on the schematic is mask $\Phi^N_{\text{mask}-r}$ and new measurement matrix A_{new} construction process.

2. Principle and methods

A schematic of the ghost imaging is shown in Fig. 1(a). The laser beam is expanded by lenses L2 and L3, projecting onto a slowly rotating ground glass to produce a pseudo-thermal light source. After passing through a beam splitter (BS), the pseudo-thermal light is divided into two paths: the probe path and the reference path. In the probe path, the probe beam goes through a transmission object $T(x)$ and the total intensity is collected by the object detector D1 (bucket detector) after passing through lens L1, recorded as I_B. In the reference path, the reference beam propagates directly to a reference detector D2 (CCD camera). The reference light intensity distribution can be recorded as $I_R(x)$ by detector D2. Then, the object image can be reconstructed by computing the intensity correlation of two light beams. In the conventional ghost imaging (GI), the second-order correlation fluctuation func-

tion is[37]

$$\Delta G^2(x) = \frac{1}{N}\sum_{i=1}^{N} I_{\mathrm{B}}^{(i)} I_{\mathrm{R}}^{(i)}(x) - \frac{1}{N}\sum_{i=1}^{N} I_{\mathrm{B}}^{(i)} \frac{1}{N}\sum_{i=1}^{N} I_{\mathrm{R}}^{(i)}(x), \quad (1)$$

where x represents the transverse spatial coordinate, $I_{\mathrm{B}}^{(i)} = \sum_x I_{\mathrm{R}}^{(i)}(x) T(x)$; $I_{\mathrm{B}}^{(i)}$ denotes the total light intensity collected by bucket detector with i-th measurement; $i = 1,2,3,\ldots,N$, and N denotes the total number of measurements; $I_{\mathrm{R}}^{(i)}(x)$ refers to the reference light intensity distributions collected by CCD in i-th measurement. The covariance of the light field at the x and x' point is defined as

$$\begin{aligned}\delta^2(x,x') &= \frac{1}{N}\sum_{i=1}^{N} I_{\mathrm{R}}^{(i)}(x) I_{\mathrm{R}}^{(i)}(x') \\ &\quad - \frac{1}{N}\sum_{i=1}^{N} I_{(R)}^{(i)}(x) \frac{1}{N}\sum_{i=1}^{N} I_{\mathrm{R}}^{(i)}(x'). \end{aligned} \quad (2)$$

Equation (1) can thus be expressed as

$$\begin{aligned}\Delta G^2(x) &= \frac{1}{N}\sum_{i=1}^{N} I_{\mathrm{B}}^{(i)} I_{\mathrm{R}}^{(i)}(x) - \frac{1}{N}\sum_{i=1}^{N} I_{\mathrm{B}}^{(i)} \frac{1}{N}\sum_{i=1}^{N} I_{\mathrm{R}}^{(i)}(x) \\ &= \frac{1}{N}\sum_{i=1}^{N}\sum_{x'}^{M} T(x')\left(I_{\mathrm{R}}^{(i)}(x') - \bar{I}(x')\right) \\ &\quad \times \left(I_{\mathrm{R}}^{(i)}(x) - \bar{I}(x)\right)\ldots \\ &\quad + \bar{I}(x)\sum_{x'}^{M}\bar{I}(x')T(x') - \frac{1}{N}\sum_{i=1}^{N} I_{\mathrm{B}}^{(i)} \frac{1}{N}\sum_{i=1}^{N} I_{\mathrm{R}}^{(i)}(x) \\ &= \delta^2(x,x)T(x) + \sum_{x'\neq x}\delta^2(x,x')T(x')\ldots \\ &\quad + \bar{I}(x)\sum_{x'}^{M}\bar{I}(x')T(x') - \bar{I}(x)\sum_{x'}^{M}\bar{I}(x')T(x') \\ &= \delta^2(x,x)T(x) + \sum_{x'\neq x}\delta^2(x,x')T(x'), \end{aligned} \quad (3)$$

where

$$\begin{aligned}&\frac{1}{N}\sum_{i=1}^{N} I_{\mathrm{B}}^{(i)} \frac{1}{N}\sum_{i=1}^{N} I_{\mathrm{R}}^{(i)}(x) = \bar{I}(x)\sum_{x}^{N}\bar{I}(x')T(x'), \\ &\bar{I}(x) = \frac{1}{N}\sum_{i=1}^{N} I_{\mathrm{R}}^{(i)}(x), \end{aligned}$$

M denotes the total number of pixels of the object, and $\delta^2(x,x)$ represents autocorrelation coefficient. $\sum_{x\neq x'}\delta^2(x',x)T(x')$ can be considered as a noise term in GI. Then DGI can be expressed as[26]

$$\begin{aligned}T(x)_{\mathrm{DGI}} &= \delta^2(x,x)T(x) + \sum_{x\neq x'}\delta^2(x,x')T(x') \\ &\quad - \bar{T}\sum_{x'}\delta(x,x'). \end{aligned} \quad (4)$$

Here, $\bar{T} = \frac{1}{M}\sum_x T(x)$.

Moreover, the reconstructed object $T(x)_{\mathrm{NGI}}^{(i)}$ by NGI in ith measurement is expressed below

$$T(x)_{\mathrm{NGI}}^{(i)} = \left(\frac{I_{\mathrm{B}}^{(i)}}{S_{\mathrm{R}}^{(i)}} - \frac{\langle S_{\mathrm{B}}\rangle}{\langle S_{\mathrm{R}}\rangle}\right)\left(I_{\mathrm{R}}^{(i)}(x) - \left\langle I_{\mathrm{R}}^{(i)}(x)\right\rangle\right), \quad (5)$$

where $\langle S_{\mathrm{B}}\rangle = (1/N)\sum_{i=1}^{N}\sum_x I_{\mathrm{B}}^{(i)}(x)$, $\langle S_{\mathrm{R}}\rangle = (1/N)\sum_{i=1}^{N}\sum_x I_{\mathrm{R}}^{(i)}(x)$, $S_{\mathrm{R}}^{(i)} = \sum_x I_{\mathrm{R}}^{(i)}(x)$, and $\langle I_{\mathrm{R}}^{(i)}(x)\rangle = (1/M)\sum_x^M I_{\mathrm{R}}^{(i)}(x)$. When measurements are enough, $\langle S_{\mathrm{B}}\rangle/\langle S_{\mathrm{R}}\rangle \approx \langle S_{\mathrm{B}}/S_{\mathrm{R}}\rangle$. Therefore,

$$\begin{aligned}T(x)_{\mathrm{NGI}} &= \frac{1}{\langle S_{\mathrm{R}}\rangle}\left(\delta^2(x,x)T(x) + \sum_{x\neq x'}\delta(x,x')T(x')\right. \\ &\quad \left. - \bar{T}\sum_{x'}\delta(x,x')\right). \end{aligned} \quad (6)$$

We can conclude from this analysis that the covariance $\delta(x,x')$ gives rise to the low SNR imaging results in GI, both DGI and NGI can suppress covariance $\delta(x,x')$ $(\sum_{x\neq x'}\delta(x,x')T(x') - \bar{T}\sum_{x'}\delta(x,x'))$ in GI to improve the quality of image. To effectively improve the quality of image better than DGI and NGI, we attempt to adopt a mask to effectively eliminate the elements $\delta(x,x')$, which are considered as correlated noise.

The speckle field of the i-th measurement is reshaped as a row vector Ψ_i of size $1\times M$. After N measurements, we can obtain an $N\times M$ measurement matrix denoted as A, which can be expressed as follows:

$$\begin{aligned}A &= \begin{bmatrix}\Psi_1\\ \Psi_2\\ \vdots\\ \Psi_{N-1}\\ \Psi_N\end{bmatrix}: \\ &= \begin{bmatrix} a_{11} & a_{12} & \cdots & a_{1(M-1)} & a_{1M}\\ a_{21} & a_{22} & \cdots & a_{2(M-1)} & a_{2M}\\ \vdots & \vdots & \ddots & \vdots & \vdots\\ a_{(N-1)1} & a_{(N-1)2} & \cdots & a_{(N-1)(M-1)} & a_{(N-1)M}\\ a_{N1} & a_{N2} & \cdots & a_{N(M-1)} & a_{NM}\end{bmatrix}. \end{aligned} \quad (7)$$

Consequently, equation (1) can be expressed as follows:

$$\begin{aligned}T_{\mathrm{GI}} &= \frac{1}{N}(A - I\langle A\rangle)^{\mathrm{T}}(A - I\langle A\rangle)T \\ &= \mathrm{cov}(A)T \\ &= \frac{1}{N}(A - I\langle A\rangle)^{\mathrm{T}}(B - I\langle B\rangle) \\ &= \frac{1}{N}A_I^{\mathrm{T}}(B - I\langle B\rangle), \end{aligned} \quad (8)$$

where $A_I = (A - I\langle A\rangle)$, T represents the transmission coefficient of the original object and is an $M\times 1$ column vector, and $B = \left[I_{\mathrm{B}}^{(1)} \cdots I_{\mathrm{B}}^{(N)}\right]^{\mathrm{T}}$. In addition, I denotes an $N\times 1$ column vector whose elements are all 1 and $\langle A\rangle$ denotes the average

of each column of A and is an $1 \times M$ row vector. Since matrix A is not an orthogonal matrix, the utilization of information is low. Under the condition of $N \gg M$, the covariance matrix $\mathrm{cov}(A)$ will approach to a diagonal matrix. This is the fundamental reason for the improvement of imaging SNR. In order to reduce the number of measurements and improve SNR, we construct a mask with OTSU method to remove the correlated noise from the covariance matrix $\mathrm{cov}(A)$. Setting $\Phi = \mathrm{cov}(A)$,normalizing matrix Φ by Eq. (9) can be expressed as follows:

$$\Phi_{\mathrm{norm}} = \frac{\Phi}{\Phi_{\mathrm{max}}}. \tag{9}$$

Here, Φ_{max} is the maximum value of the matrix Φ. Simultaneously, we need to set a valid threshold t_{m} to separate Φ_{norm} into two parts as given below.

$$\Phi^N_{\mathrm{mask}} = \begin{cases} 1 & \Phi_{\mathrm{norm}} \geqslant t_{\mathrm{m}}, \\ 0 & \Phi_{\mathrm{norm}} < t_{\mathrm{m}}. \end{cases} \tag{10}$$

We can consider that the coordinate of the element value 0 in the mask matrix Φ^N_{mask} corresponds to the position of the correlated noise in the matrix Φ. We will next describe how to set the optimal threshold t_{m} by the OTSU method.

$$\mu = \omega_0 \times \mu_0 + \omega_1 \times \mu_1, \tag{11}$$

$$g = \omega_0 \times (\mu_0 - \mu)^2 + \omega_1 \times (\mu_1 - \mu)^2, \tag{12}$$

where μ denotes the average value of the matrix Φ_{norm} and g is the variance between classes. Let K represent the number of elements of the matrix Φ_{norm}, then $K = M \times M$. The number of the parts less than t is K_0 and the average value of the corresponding elements is μ_0, the number of other parts is K_1 and the average value is μ_1, and $K = K_0 + K_1$. Moreover, $\omega_0 = K_0/K$ and $\omega_1 = K_1/K$. Through Eqs. (11) and (12), the between-class variance g can be expressed as

$$g = \omega_0 \times \omega_1 (\mu_0 - \mu_1)^2. \tag{13}$$

When the between-class variance g is maximum, we can obtain the optimal threshold t_{m}. Therefore, our method can be defined as

$$\begin{aligned} T_{\mathrm{MDGI}} &= \Phi_{\mathrm{D}} T \\ &= \Phi_{\mathrm{D}} (A - I\langle A\rangle)^{\dagger} (A - I\langle A\rangle) T \\ &= \Phi_{\mathrm{D}} A_I^{\dagger} (A - I\langle A\rangle) T \\ &= A_{\mathrm{new}} (B - I\langle B\rangle), \end{aligned} \tag{14}$$

where $\Phi_{\mathrm{D}} = \Phi^N_{\mathrm{mask}} \cdot \Phi$ ($\Phi^N_{\mathrm{mask}} \cdot \Phi$ denotes the point multiplication operation between matrices Φ^N_{mask} and Φ) and matrix $(A - I\langle A\rangle)^{\dagger}$ represents the pseudo-inverse operation of $(A - I\langle A\rangle)$. It should be noted that in our method $(1/N)A_I^{\mathrm{T}}$ is replaced by A_{new} ($A_{\mathrm{new}} = \Phi_{\mathrm{D}} A_I^{\dagger}$) compared with traditional GI method in Eq. (8). In addition, both mask Φ^N_{mask} and matrix A_{new} can be obtained through the idle reference detector measurements in engineering applications.

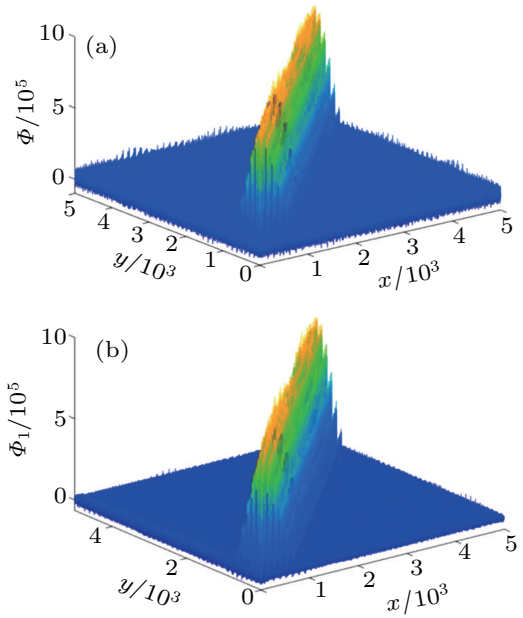


Fig. 2. Calculation results for (a) Φ and (b) Φ_1 (Φ_1 represents $A_{\mathrm{new}}A_I$), with x axis denoting row coordinate of matrix, and y axis representing column coordinate.

As a preliminary verification of the advantages of our method, we first construct matrix A_{new} through using Eq. (14). Results for Φ and Φ_1 are shown in Figs. 2(a) and 2(b), we note that the values of the off-diagonal elements in Φ are significantly greater than those in Φ_1, which explains that the correlated noise caused by off-diagonal elements in Φ is further removed.

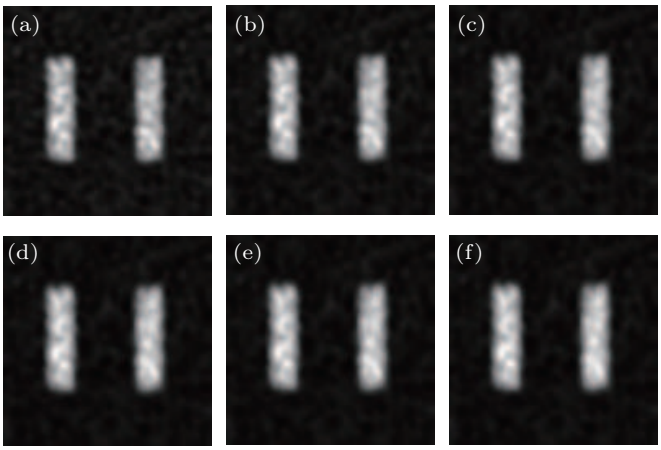


Fig. 3. Performance influence in the presence of constructed mask in MDGI, indicated by the presented reconstruction "double-slit" images all obtained from 1000 measurements. (a) MDGI image based on mask $\Phi^{1000}_{\mathrm{mask}}$; (b) MDGI image based on mask $\Phi^{1000}_{\mathrm{mask}-1}$; (c) MDGI image based on mask $\Phi^{1000}_{\mathrm{mask}-2}$; (d) MDGI image based on mask $\Phi^{1000}_{\mathrm{mask}-3}$; (e) MDGI image based on mask $\Phi^{1000}_{\mathrm{mask}-4}$; (f) MDGI image based on mask $\Phi^{1000}_{\mathrm{mask}-5}$.

Let Φ^N_{mask} and D_{r} be the sets in Z^2, then the binary dilation of Φ^N_{mask} by D_{r}, denoted as $\Phi^N_{\mathrm{mask}} \oplus D_{\mathrm{r}}$, will be defined as

the set operation:[38,39]

$$\begin{aligned}\Phi^N_{\text{mask}-\text{r}} &= \Phi^N_{\text{mask}} \oplus D_{\text{r}} \\ &= \left\{ z | \left(\hat{D}_{\text{r}}\right)_z \cap \Phi^N_{\text{mask}} \neq \emptyset \right\}, \end{aligned} \tag{15}$$

where $\oplus$ denotes the Minkowski addition and $\hat{D}_{\text{r}}$ is the reflection of the disk-shaped structuring element D_{r} with a radius of r. In other words, it is the set of element locations z, where the reflected structuring element overlaps with foreground elements in Φ^N_{mask} when translated to z.

Table 1. Reconstruction image PSNR and quality index Q based on different masks in Fig. 3.

Figure	3(a)	3(b)	3(c)	3(d)	3(e)	3(f)
r	0	1	2	3	4	5
PSNR/dB	16.3960	16.8108	16.9821	17.1008	17.1048	17.2131
Q	0.8075	0.8300	0.8404	0.8456	0.8456	0.8486

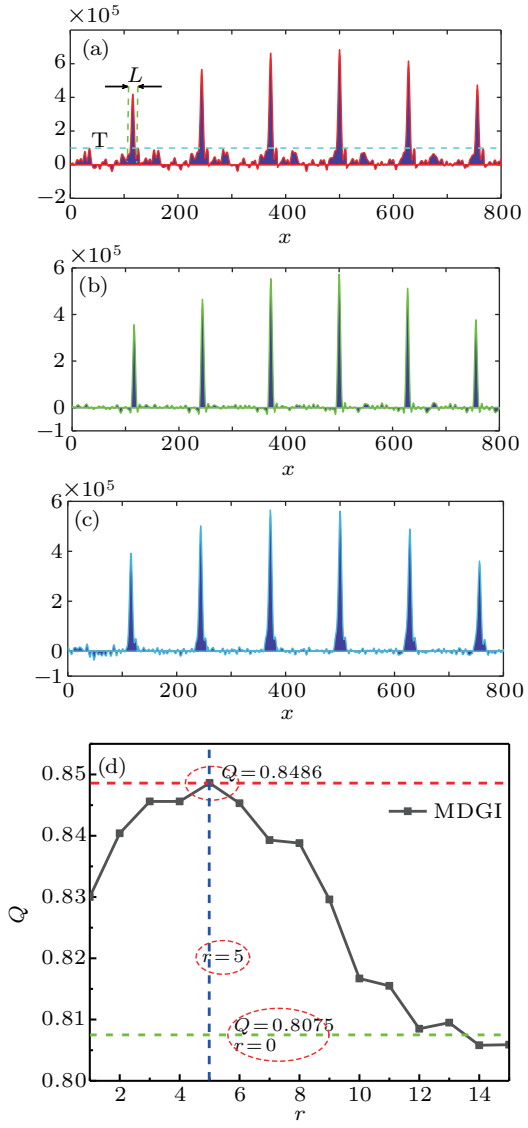


Fig. 4. (a) a row of matrix Φ ($x = 1, 2, \ldots, 800$, $y = 500$), (b) a row of matrix Φ_1 (c) a row of matrix $\left(\Phi^{1000}_{\text{mask}-5} \cdot \Phi\right) A_I^{\dagger} A_I$; (d) Q value *versus* radius r based on the results obtained in Fig. 3. The black solid curve shows the relationship between reconstruction image Q and radius r.

As shown in Fig. 4(a), we can suppress the correlated noise down to a value smaller than the threshold T ($T = \Phi_{\max} \times t_{\text{m}}$) by the mask $\Phi^{1000}_{\text{mask}}$. But accounting for correlated noise, it is likely to influence the calculation of the ideal threshold. To our knowledge, the dilation method can be used in mask $\Phi^{1000}_{\text{mask}}$ to add elements at region boundaries and to connect the disjoint parts. Thus, we try to consider modifying mask $\Phi^{1000}_{\text{mask}}$ through the dilation method to appropriately increase the width of L (L represents the number of elements whose peak value is greater than the threshold T). The elements used for imaging can be effectively retained by mask $\Phi^{1000}_{\text{mask}-5}$ results for further improving imaging quality, which is consistent with the results indicated in Table 1 and Fig. 4(d). These results demonstrate the advantage of the proposed method. However, by observing the curve in Fig. 4(d), the Q value first increases and then decreases with radius r increasing. As $r > 14$, the image quality will be lower than $r = 0$. This is mainly because when the radius $r > 5$, the constructed mask will retain more correlated noise, so that the reconstructed image quality deteriorates. Next, we will set the radius r to 5.

Let $x = \{x_i | i = 1, 2, \ldots, M\}$ and $y = \{y_i | i = 1, 2, \ldots, M\}$ be the original object image and the reconstruction image, respectively. The image quality index is defined as[31,40]

$$Q = \frac{4\delta_{xy}\bar{x}\bar{y}}{\left(\delta_x^2 + \delta_y^2\right)\left[(\bar{x})^2 + (\bar{y})^2\right]}, \quad Q \in [-1, 1], \tag{16}$$

where

$$\begin{aligned} &\bar{x} = \frac{1}{M}\sum_{i=1}^{M} x_i, \quad \bar{y} = \frac{1}{M}\sum_{i=1}^{M} y_i, \\ &\delta_x^2 = \frac{1}{M-1}\sum_{i=1}^{M} (x_i - \bar{x})^2, \quad \delta_y^2 = \frac{1}{M-1}\sum_{i=1}^{M} (y_i - \bar{y})^2, \\ &\delta_{xy} = \frac{1}{M-1}\sum_{i=1}^{M} (x_i - \bar{x})(y_i - \bar{y}). \end{aligned}$$

The best value 1 is achieved if and only if $x_i = y_i$, for all $i = 1, 2, \ldots, M$. The lowest value of -1 occurs only when $y_i = 2\bar{x} - x_i$. However, the Q value is generally not less than 0. The peak signal-to-noise ratio (PSNR) is defined as

$$\text{MSE} = \frac{1}{M}\sum_{i=1}^{M} [x_i - y_i]^2, \tag{17}$$

$$\text{PSNR} = 10 \times \log_{10}\left[\frac{\text{MAX}_I^2}{\text{MSE}}\right]. \tag{18}$$

Here, MSE represents the mean square error of the original object and the reconstructed image, and MAX_I is the maximum pixel value of the original image. The bigger the PSNR value, the better the quality of reconstruction image is.

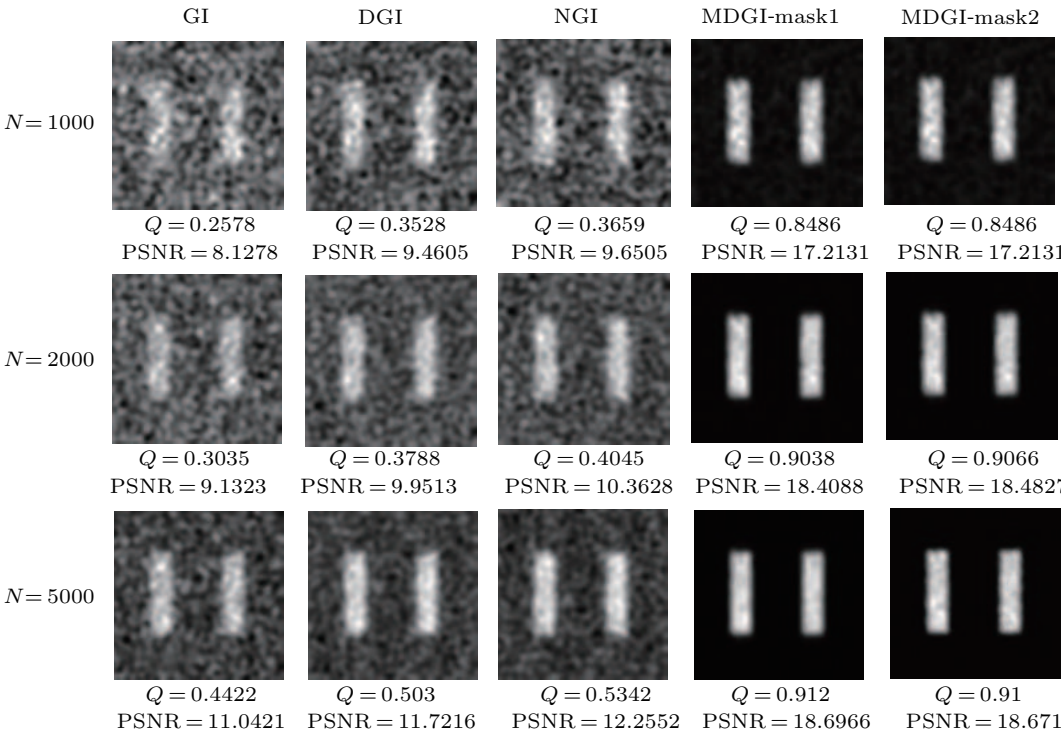


Fig. 5. Simulation results of "double-slit" with GI, DGI, NGI, MDGI-mask1, and MDGI-mask2 with N measurements.

Figure 5 displays the simulation results of "double-slit" with GI, DGI, NGI, MDGI-mask1, and MDGI-mask2 with N measurements. Figure 6 shows the curves of Q values from different methods based on the results presented in Fig. 5. We can find that the observations are consistent with the calculated quality results. The GI, DGI, NGI image are blurry due to background noise interference. Instead, our method can remove the background noise and obtain high-quality image. In addition, the performances of reconstruction quality based on different masks are demonstrated in the inset. In fact, MDGI-mask1 is the MDGI method. However, the mask2 $\Phi^{N}_{\text{mask}-5}$ is a new mask reconstructed according to the reconstruction mask procedure as the above, which is updated under different measurements. We can find that the MDGI shows almost the same performance as MDGI-mask2. In addition, The Q value of the MDGI ($N = 2000$, $Q = 0.9038$) reconstructed image is almost the same as that of MDGI ($N = 5000$, $Q = 0.912$). Therefore, we directly use mask1 $\Phi^{1000}_{\text{mask}-5}$ instead of mask2 $\Phi^{N}_{\text{mask}-5}$ and the number of measurements is set to 2000 to avoid extra calculations in this paper.

As shown in Figs. 7(a) and 7(b), the object can hardly be distinguished from GI images. Although the DGI and NGI reconstructed images are better than GI, the PSNR and Q value of the reconstructed image are still too low due to the interference by background noise, which is also consistent with the visual observation. However, the reconstructed image obtained by MDGI can effectively remove the background noise, and the obtained image has the higher PSNR value and Q value. It should be noted that the MDGI uses the dilation method and the MDGI1 does not, and finally the MDGI gets better results than the MDGI1. Meanwhile, the Q-fitting curves from the five methods with different numbers of measurements are shown in Figs. 8(a) and 8(b). It can be observed that the MDGI obtains a higher Q value than the other methods under the same number of measurements. This implies that our method is not only suitable for binary objects but is also suitable for complicated objects.

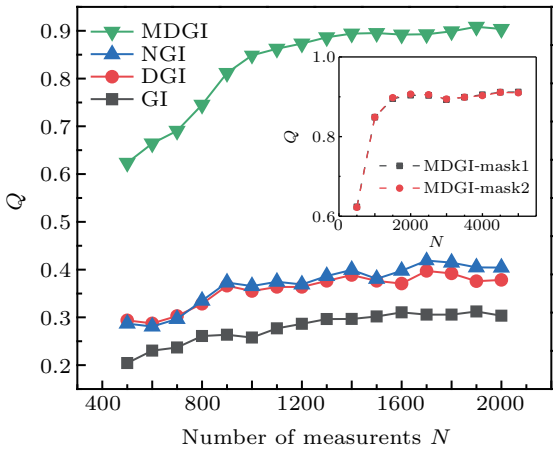


Fig. 6. Relationships between the number of measurements and Q value for reconstructed binary image "double-slit" under different GI methods. Inset indicates the comparison between MDGI based on the same mask1 $\Phi^{1000}_{\text{mask}-5}$ and that based on the varying mask2 $\Phi^{N}_{\text{mask}-5}$ under different measurements. Solid curve with pentagrams shows MDGI reconstruction results. Solid curve with circles and solid curve with triangles correspond to DGI and NGI reconstruction results, respectively. Curve with squares refers to GI reconstruction results.

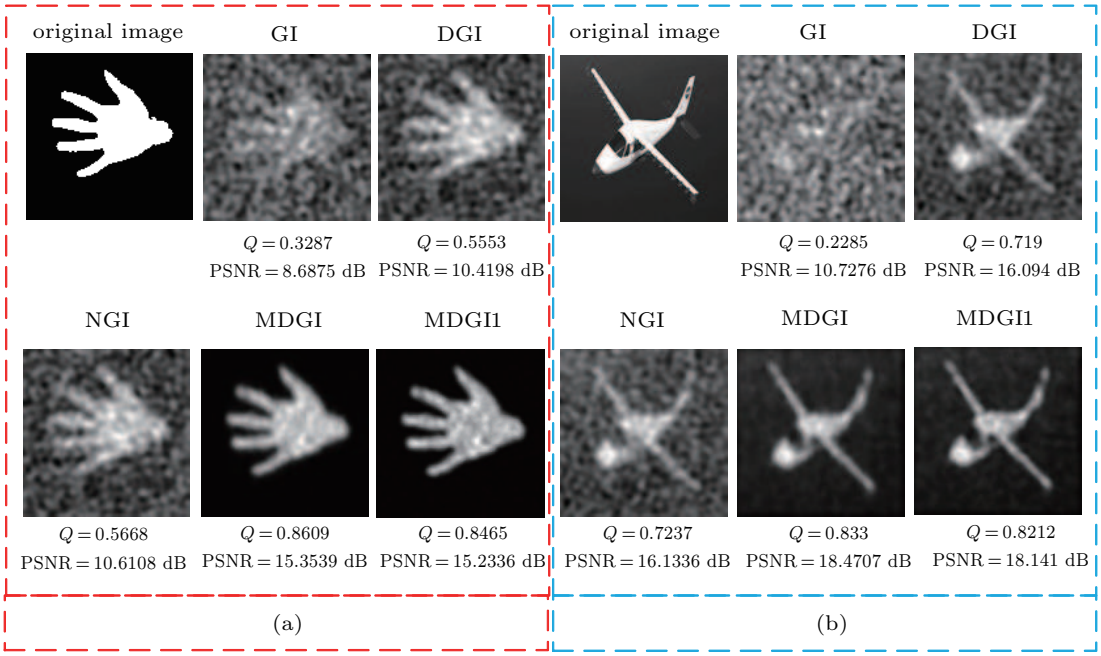


Fig. 7. Simulation results of traditional GI, DGI, NGI, MDGI, and MDGI1 with 2000 measurements. (a) Simulation results of binary image "palm". (b) Simulation results of grayscale image "aircraft".

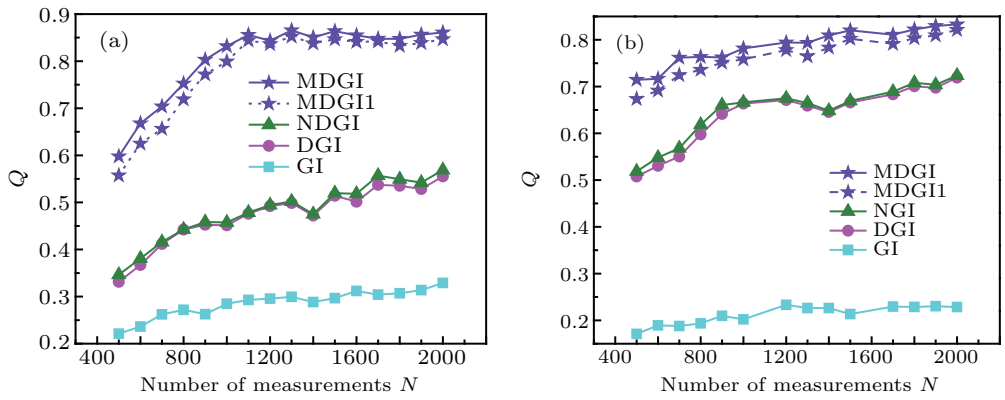


Fig. 8. Plots of Q value *versus* the number of measurements based on different reconstruction methods, based on the results obtained in Fig. 7. Curves in panels (a) and (b) are the reconstruction results of "palm" and "aircraft", respectively. Solid curves and dashed curves with pentagrams show the performance of MDGI with $\Phi^{1000}_{\text{mask}-5}$ and MDGI1 with Φ^{N}_{mask}, respectively. Solid curves with rounds and triangles correspond to the DGI and NGI reconstruction result, respectively. Curve with squares indicates the GI reconstruction results.

3. Experimental results and analysis

To put our method into practice, we make an experimental system according to the experimental schematic in Fig. 1(a). The He–Ne laser beam (with wavelength $\lambda = 532$ nm) is expanded by L2 and L3, passing through the slowly rotating glass disk and producing randomly varying speckle fields. After a BS, the pseudo-thermal light is divided into two beam arms: reference arm and detection beam. In the reference arm, the reference beam is directly collected by detector D2 (CCD: Stingray F-504, AVT, Germany) and the resolution is approximately 3.45 μm×3.45 μm. In the detection arm, the beam goes through the digital mask letter "GI" with 128×128 pixels and expands after L1, the total light intensity is collected by detector D1. In the experiment, we use the same type of CCD as a bucket detector and sum the light intensity distributions to obtain total light intensity. Here $z_1 = z_2 = 200$ mm, $f = 150$ mm. The personal computer used for reconstruction image is an ASUS desktop machine (CPU: Intel core is i7-7700, 3.60 GHz, 16 GB). The total number of measurements is 2000. Figure 9 shows the experimental results obtained from different GI methods. Figure 9(a) displays the original image of the digital mask. Figure 9(b) exhibits the reconstruction image through traditional GI. Figures 9(c) and 9(d) show the reconstruction results obtained by using the DGI and the NGI, respectively. Figure 9(e) shows the MDGI image. However, the reconstruction images by the GI, DGI, and NGI are blurry. Unlike the above methods, our method can effectively remove background noise and obtain the robust image. The Q value of MDGI image is increased by 0.2915 compared with that obtained from the NGI, and the PSNR is increased by 5.1265 dB.

The Q value of the MDGI method is higher than that of the MDGI1 method for a given number of measurements as shown in Fig. 10. In the case of 2000 measurements, the Q for MDGI exceeds that for MDGI1 by as high as 0.11. From these results, it can be concluded that the proposed method is robust and feasible to be implemented in the practical engineering application.

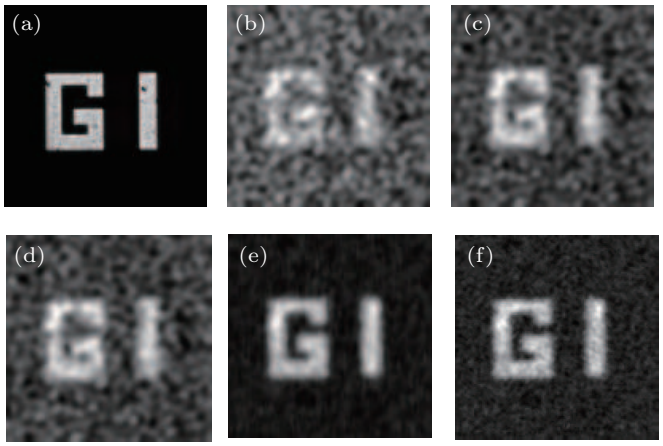


Fig. 9. Experimental results for 2000 measurements. (a) Original object; (b) traditional GI image, PSNR = 9.3702 dB and $Q = 0.2624$; (c) DGI image, PSNR = 11.3125 dB and $Q = 0.3651$; (d) NGI image, with PSNR = 11.4031 dB and $Q = 0.3738$; (e) MDGI image, PSNR = 16.5296 dB and $Q = 0.6653$; (f) MDGI1 image, PSNR = 14.8747 dB and $Q = 0.5535$.

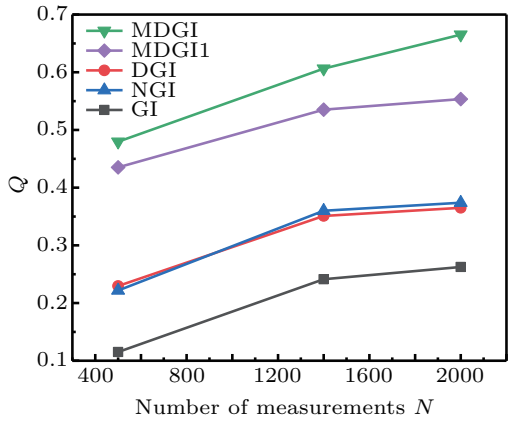


Fig. 10. Relationships between the number of measurements and Q reconstruction image "GI" for different GI methods. Green solid curve with triangles represents MDGI. Purple solid curve with diamonds is for MDGI1. Red and blue solid curve with solid circles and triangles refer to DGI and NGI reconstruction results respectively. Black solid curve with squares is for GI reconstruction results.

4. Conclusions

In this work, we have demonstrated the performance of MDGI through experimental and numerical simulations. We first theoretically analyze the influence of correlated noise in GI. A novel denoising model is thereafter proposed to remove the correlated noise in GI through a mask. Furthermore, the mask construction can be obtained by the idle reference detector measurements. Simulation and experimental results show that the reconstruction image quality from the proposed method is better than those from the GI, DGI, and NGI. This research provides an alternative way to the correlated noise suppression, which is also applicable to the fields of biological imaging, lidar, and so on.

References

[1] Klyshko D N 1988 *Sov. Phys. JETP* **67** 1131
[2] Pittman T B, Shih Y H, Strekalov D V and Sergienko A V 1995 *Phys. Rev. A* **52** R3429
[3] Bennink R S, Bentley S J and Boyd R W 2002 *Phys. Rev. Lett.* **89** 113601
[4] Si Y, Kong L J, Li Y N, Tu C H and Wang H T 2016 *Chin. Phys. Lett.* **33** 034203
[5] Cao D Z, Li Q C, Zhuang X C, Ren C, Zhang S H and Song X B 2018 *Chin. Phys. B* **27** 123401
[6] Zhang D, Zhai Y H, Wu L A and Chen X H 2005 *Opt. Lett.* **18** 2354
[7] Cheng J 2009 *Opt. Express* **17** 7916
[8] Meyers R E, Deacon K S and Shih Y 2012 *Appl. Phys. Lett.* **100** 131114
[9] Shi D, Fan C, Zhang P, Shen H, Zhang J, Qiao C and Wang Y 2013 *Opt. Express* **21** 2050
[10] Cheng J and Lin J 2013 *Phys. Rev. A* **87** 043810
[11] Gong W and Han S 2011 *Opt. Lett.* **36** 394
[12] Tian N, Guo Q, Wang A, Xu D and Fu L 2011 *Opt. Lett.* **36** 3302
[13] Chen W and Chen X 2014 *Appl. Phys. Lett.* **104** 251109
[14] Zhao C, Gong W, Chen M, Li E, Wang H, Xu W and Han S 2012 *Appl. Phys. Lett.* **101** 141123
[15] Li X, Deng C, Chen M, Gong W and Han S 2015 *Photon. Res.* **3** 153
[16] Yang X, Zhang Y, Xu L, Yang C H, Wang Q, Liu Y H and Zhao Y 2015 *Chin. Phys. B* **24** 124202
[17] Gong W, Zhao C, Yu H, Chen M, Xu W and Han S 2016 *Sci. Rep.* **6** 26133
[18] Li Z, Suo J, Hu X and Dai Q 2016 *Opt. Express* **24** 7328
[19] Ryczkowski P, Barbier M, Friberg A T, Dudley J M and Genty G 2016 *Nat. Photon.* **10** 167
[20] Zhang Y and Zhao S 2017 *Chin. Phys. B* **26** 054205
[21] Li H X, Bai Y F, Shi X H, Nan S Q, Qu L J, Shen Q and Fu X Q 2017 *Chin. Phys. B* **26** 104204
[22] Wang C, Mei X, Pan L, Wang P, Li W, Gao X and Han S 2018 *Remote Sens.* **10** 732
[23] Wang L, Zou L and Zhao S 2018 *Opt. Commun.* **407** 181
[24] Sun B, Welsh S S, Edgar M P, Shapiro J H and Padgett M J 2012 *Opt. Express* **20** 16892
[25] Ferri F, Magatti D, Lugiato L A and Gatti A 2010 *Phys. Rev. Lett.* **104** 253603
[26] Yao X R, Yu W K, Liu X F, Li L Z, Li M F, Wu L A and Zhai G J 2014 *Opt. Express* **22** 24268
[27] Li G, Yang Z, Zhao Y, Yan R, Liu X and Liu B 2017 *Laser Phys. Lett.* **14** 025207
[28] Zhou Y, Zhang H, Zhong F, Guo S X 2018 *Acta Phys. Sin.* **67** 244201 (in Chinese)
[29] Zhao S M and Zhuang P 2014 *Chin. Phys. B* **23** 054203
[30] Wu H, Zhang X, Gan J, Luo C and Ge P 2016 *Laser Phys. Lett.* **13** 115205
[31] Zafari M, Ahmadi-Kandjani S, Kheradm and R 2017 *Opt. Commun.* **387** 182
[32] Shi X, Huang X, Nan S, Li H, Bai Y and Fu X 2018 *Laser Phys. Lett.* **15** 045204
[33] Zhang C, Guo S, Cao J, Guan J and Gao F 2014 *Opt. Express* **22** 30063
[34] Gong W 2015 *Photon. Res.* **3** 234
[35] Yang C, Wang C, Guan J, Zhang C, Guo S, Gong W and Gao F 2016 *Photon. Res.* **4** 281
[36] Otsu N 1979 *IEEE Trans. Syst. Man Cybern* **9** 62
[37] Zerom P, Shi Z, O'Sullivan M N, Chan K W C, Krogstad M, Shapiro J H and Boyd R W 2012 *Phys. Rev. A* **86** 063817
[38] Boomgaard R V D and Balen R V 1992 *CVGIP: Graphical Models Image Process.* **54** 252
[39] Adams R 1993 *CVGIP: Graphical Models Image Process.* **55** 325
[40] Wang Z and Bovik A C 2002 *IEEE Signal Process. Lett.* **9** 81